Global and Planetary Change 221 (2023) 104042

Contents lists available at ScienceDirect

Global and Planetary Change

journal homepage: www.elsevier.com/locate/gloplacha

Ice volume variations and provenance trends in the Oligocene-early Miocene glaciomarine sediments of the Central Ross Sea, Antarctica (DSDP Site 270)

Valerio Olivetti [a,*], Maria Laura Balestrieri [b], David Chew [c], Luca Zurli [d], Massimiliano Zattin [a], Donato Pace [d], Foteini Drakou [c], Gianluca Cornamusini [d,e], Matteo Perotti [d]

[a] Geosciences Department, University of Padova, Padova, Italy
[b] Consiglio Nazionale delle Ricerche, Istituto di Geoscienze e Georisorse, Sede di Firenze, Firenze, Italy
[c] Department of Geology, Trinity College Dublin, The University of Dublin, Dublin 2, Ireland
[d] Department of Physical, Earth and Environmental Sciences, University of Siena, Siena, Italy
[e] Museo Nazionale dell'Antartide, Sezione di Siena, Siena, Italy

ARTICLE INFO

Editor: Dr. Alan Haywood

Keywords:
Provenance analysis
Apatite and zircon U-Pb dating
Antarctica
Ice-sheet evolution
Late Oligocene glacial event
DSDP Site 270

ABSTRACT

Since the early Oligocene, the descent into global colder conditions has led to the stepwise growth of the Antarctic Ice Sheets. However, ocean and air temperatures were not sufficiently cold enough to maintain a large and stable continental ice sheet and associated marine ice shelf, and therefore during the Oligocene to Miocene the glaciation waxed and waned. However there is limited geological evidence for the extent of these early glacial episodes. Here we present a multi-proxy single-grain provenance study on the glaciomarine sediments in DSDP Site 270, from the Central High in the central Ross Sea to determine the extent of such ice volume variations.

The Ross Sea embayment is a key region in Antarctica for preserving geological evidence on the early glacial events, because glaciation was synchronous with continuous sea-floor subsidence and uplift of the surrounding mountain ranges. The Central High in the central Ross Sea was drilled by the DSDP project in the 1970s (Site 270) and a sequence of c. 400 m of Oligocene to lower Miocene glaciomarine sediments was recovered, underlain by a few meters of granitic talus breccia and gneissic basement rocks. The sediments evolve from a non-glacial, continental environment to a glaciomarine environment characterized by variable ice-rafted debris content and several diamictite units. Our approach combines information on crystallization ages in the source region (U-Pb detrital zircon dating), medium- and low-temperature thermochronology constraints (detrital apatite U-Pb and fission-track dating on the same grains), information on the source bedrock type (detrital apatite trace element analysis) and petrological analysis of gravel-size clasts. We provide new constraints on the ice sheet evolution since the earliest phases of glaciation, and show a transition from local to regional-scale ice sheets in the central Ross Sea region in the late Oligocene and early Miocene. In addition, our data can identify the source of sediment transported by ice streams to the central Ross Sea from different areas in the Transantarctic Mountains (TAM) and within the West Antarctic Rift System (WARS). In particular, the provenance data show the late Oligocene diamictite strata were sourced from a distant region, likely southern West Antarctica, indicating a substantial continental ice sheet already existed in the late Oligocene. These new data provide robust geological constraints for modeling of ice sheet volumes and ice drainage patterns in the late Oligocene-early Miocene.

1. Introduction

The sediments of the Ross Sea Embayment, the southernmost sea on Earth, can in many ways be regarded as a book which tells the story of the tectonic and climate history of this segment of Antarctica in the last 34 million years. The pages of this book are the marine and glacial sediments, accumulated in a subsiding and extending marine basin surrounded on three sides by land. The words of this book are the detritus (mineral grains and clasts) eroded from the surrounding Antarctic bedrock and transported by glaciers, marine currents and icebergs

* Corresponding author.
E-mail address: valerio.olivetti@unipd.it (V. Olivetti).

https://doi.org/10.1016/j.gloplacha.2023.104042
Received 12 June 2022; Received in revised form 19 December 2022; Accepted 11 January 2023
Available online 18 January 2023

to the basin. Each grain tells the history about the geological events in the source area and when integrated, this provenance analysis yields information on the environmental conditions that influenced the mechanisms of transport. The specific history told here is recorded in a marine record drilled in 1973 by the DSDP drilling project (Leg 28 Site 270) that covers a period of c. 6 myr, between 26 and 20 Ma (Shipboard Scientific Party, 1975; Leckie and Webb, 1983; Kulhanek et al., 2019). During this period, the Central High (Fig. 1), a topographic high that emerged above sea level before 26 Ma and located in the middle of the Ross Embayment, recorded two key transitions in sedimentary facies and climate: a shift from continental to marine conditions followed by a transition from non-glacial to glacial conditions.

The geological history of the Central Ross Sea is based primarily on data acquired through a series of seismic campaigns that have identified repeated glacial events since the early Miocene, starting with the nucleation of small terrestrial glaciers and ice caps that developed into a larger ice sheet (De Santis et al., 1995). Recently, the central Ross Sea region has been the focus of renewed studies on the early glacial history of Antarctica: the age model of the DSDP Site 270 legacy core has been revised and improved (Kulhanek et al., 2019), new sea surface paleotemperature data based on membrane lipid distributions from archaea have been determined from DSDP site 270 (Duncan et al., 2022) and a recent IODP drilling campaign (site U1521) has been carried out (McKay et al., 2019).

In this work we address the topical Oligocene to Miocene tectonic and environmental evolution of the Ross Sea region by using an integrated single-grain provenance approach. This multi-proxy provenance study employs conventional U-Pb detrital zircon dating integrated with apatite U-Pb and fission-track dating and trace element analysis of detrital apatite and clast petrology. Recent advances in U-Pb dating of

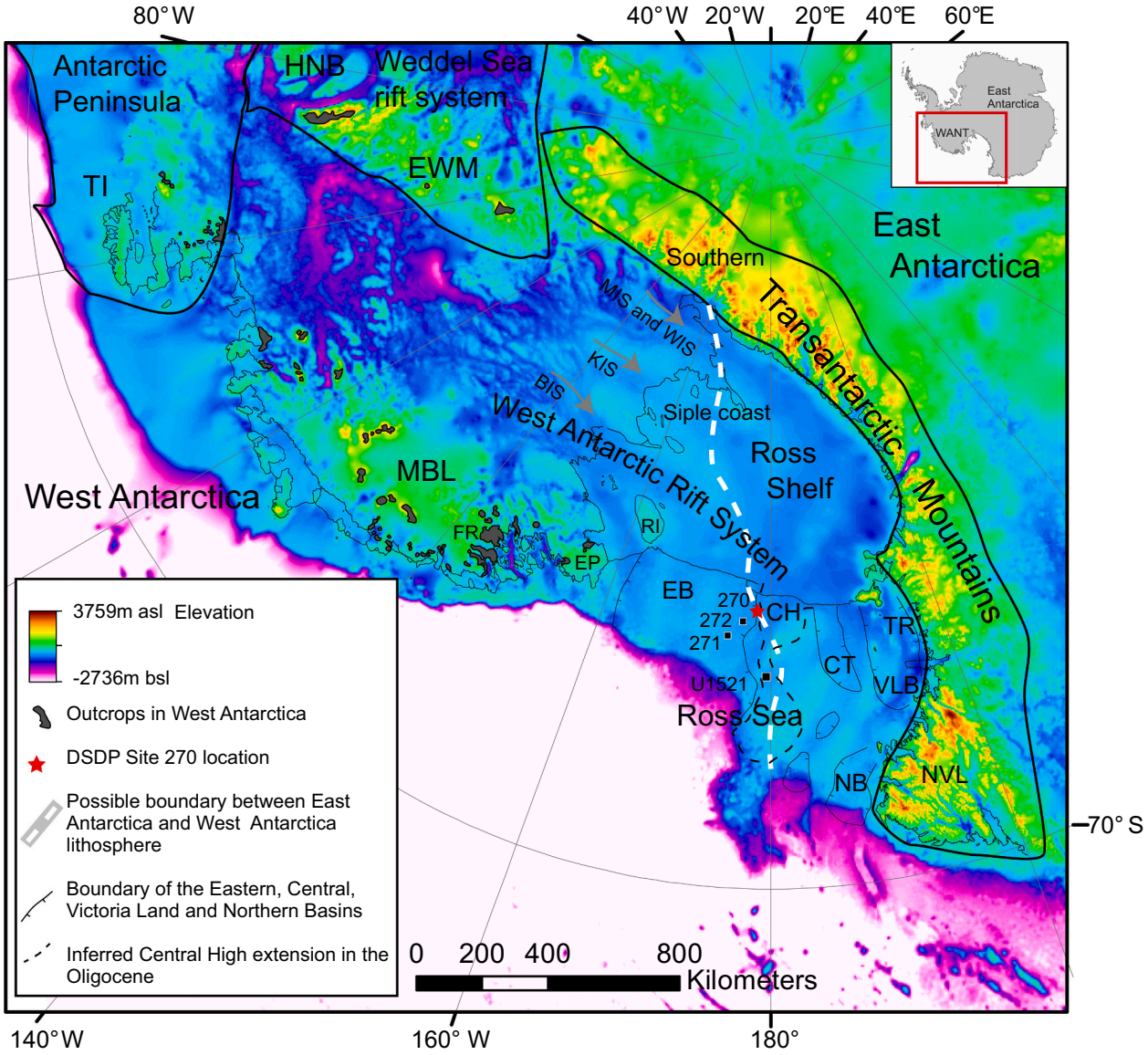

Fig. 1. Ross Sea region subglacial topography and bathymetry from Bedmap2, derived from geophysical data (Fretwell et al., 2013). The thick black lines demarcate geotectonic provinces (modified from Jordan et al., 2020). Rocks that crop out in West Antarctica are shown in dark grey. Outcrops in the TAM (which are well exposed) are not shown. The white dashed line represents the inferred boundary between the West and East Antarctica lithosphere (Tinto et al., 2019). Sedimentary basins redrawn from Davey and Brancolini (1995); the Oligocene extension of the Central High is from De Santis et al., 1995. HNB: Haag Nunataks Block; TI, Thurston Island; EWM, Ellsworth-Whitmore Mountains; WIS, Whillans Ice Stream; MIS, Mercer Ice Stream; KIS Kamb Ice stream; BIS, Bindschadler Ice Stream; MBL, Marie Byrd Land; FR, Ford Ranges; EP, Edward VII Peninsula; RI, Roosevelt Island; EB, Eastern Basin; CH, Central High; CB, Central Basin; VLB, Victoria Land Basin; TR, Terror Rift; NB, Northern Basin; NVL, northern Victoria Land.

common Pb-bearing minerals and linking detrital apatite trace element composition to source rock lithology have substantially improved the application of detrital apatite as a provenance proxy (O'Sullivan et al., 2016; O'Sullivan et al., 2018).

Geochronology as provenance tool of glacigenic sediment is largely used in the Ross Sea where diagnostic ages can identify a provenance from proximal vs far away or West Antarctica (WA) vs East Antarctica (EA) sources with implication on the ice flow pattern, ice volumes and erosional history of the source area (e.g Licht et al., 2014; Licht and Hemming, 2017; Perotti et al., 2017). Recently Marschalek et al. (2021) employed detrital geochronology, neodymium and strontium isotope compositions to infer an early Miocene expansion of the West Antarctic Ice Sheet (WAIS), whose evolution through time is considered very important for both global climate and to reconcile its growth history with the far-field oxygen isotope deep sea record (e.g. Naish et al., 2022).

Our detrital geochronology data suggest a general evolution from locally sourced sediments to far-travelled glacial detritus in agreement with a continuous sea floor subsidence seen in seismic lines (De Santis et al., 1995, 1999), and with paleotopographical reconstructions (Paxman et al., 2019; Pollard and DeConto, 2020). Importantly in this study, the detrital age spectra of a late Oligocene diamictite contains far-travelled grains from southern WA, documenting the earliest unrecorded expansion of the WAIS.

2. Age and lithology of the Ross Sea bedrock

Because the provenance data presented in this study concern (apatite and zircon) U-Pb ages and apatite fission-track (AFT) exhumation histories in the sediment source area(s), we summarize here i) the main geological events in the regional crystalline basement, ii) sedimentary sequences that could potentially be a source of detrital apatite and zircon (i.e. recycling) and iii) regional shallow crustal erosion as recorded by AFT data.

Most of the crystalline rocks cropping out around the Ross Sea Embayment formed during Neoproterozoic and Phanerozoic orogenic events associated with the subduction and convergence of the Paleo-Pacific plate (Stump, 1995; Veevers, 2004; Goodge, 2020; Jordan et al., 2020).

Several sedimentary basins developed on top of this basement in a variety of tectonic settings spanning from active-margin to intracratonic and foreland type. In particular, in the TAM, the basement was covered by a thick series of continental sediments and magmatic products of the Ferrar Large Igneous Province (Elliot, 2013; Jordan et al., 2020).

Since the Cretaceous, a predominantly extensional tectonic regime led to the formation of the West Antarctic Rift System (WARS) that resulted in the partial separation of WA from the East Antarctica (EA) (Siddoway, 2008; Behrendt, 1999). Today, the West Antarctica bedrock is largely hidden below ice cover with most of the sparse outcrops exposed in Marie Byrd Land (MBL) (Fig. 1).

2.1. Pre-Ross Orogeny events

Evidence for Mesoproterozoic orogenesis associated with the formation of the Rodinia supercontinent (Grenville Orogeny sensu *latu*) is found only in the Haag Nunatak block, between the WARS and the Antarctica Peninsula (Fig. 1)(Millar and Pankhurst, 1987). However, the detrital record of Mesoproterozoic orogenesis is recorded by late Neoproterozoic-early Paleozoic metasedimentary sequences (meta-turbidites) (Goodge et al., 2004; Paulsen et al., 2015; Estrada et al., 2016) that were in turn recycled and became the main source of Grenvillian-aged detritus within Cenozoic deposits (Marschalek et al., 2021).

2.2. Ross Orogeny

Rocks associated with the Ross Orogeny crop out primarily in the TAM, while Ross Orogeny rocks are very limited in MBL, with a solitary pluton dated at 505 Ma (Jordan et al., 2020). The Ross Orogeny belt formed in the latest Neoproterozoic to early Paleozoic times, along an active convergent plate margin of Gondwana. Ross Orogeny convergence resulted in marginal-basin development, high- to low-grade metamorphism and volumetrically significant calc-alkaline granitoid batholiths (see Goodge, 2020 for a review). The age of emplacement of granitoids spans the Cambrian through to the Ordovician with the main magmatic phase dated at 520–480 Ma, although older detrital igneous zircons in *syn*- to post-orogenic siliciclastic rocks imply that magmatism was underway by at least c. 600 Ma (Goodge, 2020, Paulsen et al., 2015). Detritus associated with the Ross Orogeny is found within the late Cambrian-Ordovician low-grade metaturbidites of the Swanson Formation (WA) and Robertson Bay Formation and Byrd Group (EA), as well as syn-Ross Orogeny metasedimentary formations of the TAM (i.e., the Beardmore Group, Skelton Group, and Wilson Group) (Goodge et al., 2004; Paulsen et al., 2015; Di Vincenzo et al., 2014; Estrada et al., 2016). The Ross Orogeny age is a common population within the late Paleozoic-Mesozoic sedimentary sequences cropping out in the TAM (Elsner et al., 2013; Elliot et al., 2015; Zurli et al., 2022a).

2.3. Lachlan orogeny, Devonian-Carboniferous

This orogenic phase is represented by the Ford Granodiorite, a series of calc-alkaline plutons associated with a convergent margin and now exposed in eastern MBL (Pankhurst et al., 1998; Siddoway, 2008; Yakymchuk et al., 2015). Similar magmatic bodies are exposed along the TAM in northern Victoria Land (Admiralty Intrusives and Gallipoli Volcanics) (Goodge, 2020).

Devonian-Carboniferous U-Pb ages (370–340 Ma) have been reported by McFadden et al. (2010) from zircon cores from a Cretaceous gneiss (Fosdick Mountains, MBL). An early Silurian age (437 Ma) has been found by Mortimer et al. (2011) in the gneiss at the base of the DSDP 270 drill core (U-Pb on titanite), suggesting that portions of the WARS and WA were involved in the early stage of the Lachlan Orogeny.

2.4. Permo-Triassic and Jurassic volcanism

Permo-Triassic magmatic and metamorphic rocks associated with the Andean-type Gondwanide orogeny are found from South America through Antarctica (MBL and the Ellsworth-Whitmore Mountains, EWM, Fig. 1) through to New Zealand. Triassic granites are exposed in the EWM. In the TAM, Triassic volcanic detritus is found also within the Triassic sandstones of the Beacon Supergroup (a sedimentary formation of mainly continental facies extensively exposed along the TAM) (Elliot et al., 2017, 2019; Paulsen et al., 2017). A major Early Jurassic magmatic pulse related to a Large Igneous Province occurred at the end of this orogenic phase. This magmatic event includes the emplacement of the Ferrar mafic igneous province around 183–182 Ma along EA, represented by dolerites and basalts (Burgess et al., 2015).

2.5. Cretaceous magmatism and extension

Cretaceous rocks are exposed in the MBL and absent in the TAM (Fig. 1). They are associated with magmatism and deformation associated with back-arc extension of the Phoenix (paleo-Pacific) plate that marks the shift from convergence to extension, induced by a possible slab retreat (see Jordan et al., 2020 for a review). The lithologies associated with this event are calc-alkaline arc plutons and broadly coeval migmatitic gneisses that were exhumed by crustal-scale detachment faults.

2.6. Cenozoic - renewed WARS extension and TAM uplift/erosion

During the Eocene-Oligocene, crustal extension within the WARS resumed, particularly in the western Ross Sea with the rapid development of a narrow rift (Victoria Land Basin and later Terror Rift, Fig. 1), synchronous to the main phase of uplift and consequent erosion of the TAM (Fitzgerald, 1992). This renewed extension triggered alkaline volcanism in Victoria Land (EA) and Marie Byrd Land, that commenced in the Eocene with the largest volcanic edifices developing in the mid-Miocene onwards (Rocchi et al., 2002; LeMasurier, 2013).

2.7. Detrital age spectra in Ross Sea sediments

The recent provenance study of Marschalek et al. (2021) on Miocene sediments from the central Ross Sea shows that the U-Pb zircon peak corresponding to the Ross Orogeny is always present and dominant, while the occurrence of Triassic and Cretaceous U-Pb zircon populations coupled with palynological, neodymium isotope data from mudrocks and petrographic data on clasts, indicate WA provenance. Several U-Pb detrital zircons studies undertaken on Quaternary sediments of the central Ross Sea, have shown that the Ross Orogeny U-Pb zircon peak is always the dominant population (Licht and Palmer, 2013; Licht et al., 2014; Licht and Hemming, 2017; Perotti et al., 2017). In these studies, Cretaceous U-Pb zircon ages are very rare while rare Triassic U-Pb zircon ages are considered as reworked magmatic zircon derived from Triassic Beacon Supergroup sandstones.

Detrital AFT ages in Quaternary sediments from the eastern, central and western Ross Sea reflect the age of erosion of the source rocks. In general, the dominant population corresponds to a long-lasting erosion event during the Cretaceous that is common to both WA and the TAM (Perotti et al., 2017; Li et al., 2020). Eocene-Oligocene exhumation is also detected in the Quaternary sediments from the entire Ross Sea; these young AFT ages imply fast erosion that is uniquely associated with a TAM provenance (Fitzgerald, 2002; Olivetti et al., 2013).

3. Stratigraphy of the DSDPLeg 28, Site 270 borehole

DSDP Site 270 drill hole penetrated 422.5 m below sea floor with a 60% core recovery (Shipboard Scientific Party, 1975)(Fig. 2a). At the bottom, the core contains 9 m of metasedimentary basement rock composed of calc-silicate and marble overlain by 26 m of sedimentary breccia made of metasedimentary and granite clasts, inferred to represent a talus deposit with evidence of subaerial weathering (Shipboard Scientific Party, 1975). A calcareous glauconitic sandstone (1 m thick) and carbonaceous quartz sand with woody fragments (2 m) overlie the talus and represent a non-glacial sequence (Shipboard Scientific Party, 1975; Leckie and Webb, 1983). Above these sandstones, a thick sequence of glaciomarine deposits (363 m) of mostly mudstone with varying amounts of ice rafted debris (IRD) is present. Recent work (Kraus, 2016) highlighted new lithostratigraphic characteristics based on IRD and mud content (Fig. 2a): sediments between 385 and 348 mbsf are dominated by sandstones, followed by mudstones with a constant amount of IRD (c. 3%) between 348 and 252 mbsf. Above, there is a sequence of massive and stratified diamictite, interlayered with mudstone with dropstones, sandstone and siltstone beds (252 to 202 mbsf). The deposits above between 202 and 20 mbsf are dominated by mudstones with absent to rare clasts in the lowest portion and with dispersed and common IRD above ca. 125 mbsf with several levels of thin diamictites. The uppermost ~20 mbsf overlies a major unconformity and consists of Pliocene to recent glacial deposits.

4. Methods

All U-Pb and trace element analyses of apatite and zircon were undertaken using a Photon Machines Analyte Exite ArF Excimer laser-ablation system coupled to an Agilent 7900 at Trinity College Dublin. The U-Pb apatite method is a medium-temperature thermochronometer with a temperature sensitivity between 350° and 570 °C (Chew and Spikings, 2021), thus making this technique a powerful tool to study crystallization and subsequent cooling in metamorphic belts. The U-Pb dating technique is affected by the variable (and often significant) common Pb in apatite making this method particularly challenging in dating low-uranium detrital grains where multiple dating of cogenetic grains is not possible.

In this study we followed the procedures given by Chew et al. (2014), which employs the VizualAge_UcomPbine data reduction scheme (DRS), a modification of the U-Pb geochronology "VizualAge" DRS of Petrus and Kamber (2012) that can account for the presence of variable common Pb in the primary standard materials. The DRS runs within the freeware IOLITE package of Paton et al. (2011). Common Pb correction in the unknowns employs a starting estimate for the age of the unknown, calculating its corresponding $^{207}Pb/^{206}Pb$ initial ratio using the Stacey and Kramers (1975) terrestrial Pb-evolution model and then adopting an iterative approach based on a ^{207}Pb correction (Chew et al., 2011). All grains with ^{207}Pb-corrected 2σ age uncertainties of either >25% or > 100 myr were therefore excluded, following the procedure of Mark et al. (2016).

U-Pb dating of detrital zircon is a routine tool in single-grain provenance studies, including Antarctic glacigenic sediments (e.g. Licht et al., 2014; Licht and Hemming, 2017). This is because of the refractory behavior of zircon, its high U and very low initial Pb concentrations, and its high closure temperature of >900 °C (Cherniak and Watson, 2001). Zircon data reduction employed the "VizualAge" DRS of Petrus and Kamber (2012).

Apatite trace element (including REE) compositions were interrogated using the approach of O'Sullivan et al. (2020) that uses a Support Vector Machine (SVM) categorization to compare apatite unknowns with a comprehensive database of apatite-bedrock pairs. Bedrock categorization is achieved using a plot of apatite Sr/Y ratio versus the sum of the light REE (defined as La-Nd). Apatite U-Pb and trace element analyses were undertaken during the same ablation.

The apatite fission-track (AFT) method is a well-established low temperature thermochronology technique that is sensitive to shallow crustal temperatures between 60 °C and 120 °C (the apatite Partial Annealing Zone or PAZ, Gleadow and Duddy, 1981). When AFT thermochronology is undertaken on apatite detritus that has not undergone post-depositional heating above the thermal sensitivity of the system, we obtain a single-grain age distribution which reflects the thermal history and exhumation of the source region(s) which can also yield information on sedimentary provenance and the regional landscape evolution (Bernet et al., 2004; Brandon et al., 1998). All apatite grains dated by the AFT technique in this study employed the external detector method and subsequently underwent combined U-Pb and trace element analysis by LA-ICP-MS.

Petrology and distribution of clasts has been successfully employed in provenance studies in the Ross Sea region both from offshore and onshore glacigenic deposits (e.g. Talarico and Sandroni, 2011; Talarico et al., 2012; Perotti et al., 2018). In this study the petrology and relative abundance of clasts (>2 mm) in the sedimentary sequence were evaluated on the archived half sections of the core held at the IODP Gulf Coast Repository in Texas A&M University, College Station (USA). Clasts were grouped into seven different lithologies based on macroscopic and microscopic petrography following Zurli et al. (2022b).

5. Results

We analyzed ten samples from the DSDP Site 270 record. Eight are detrital samples composed of 250 cc of glaciomarine sediments distributed along the core and two (one from a granite clast occurring in the basal talus breccia and one from the basal calc-silicate gneiss) come from the basement rocks recovered during coring. For six glaciomarine sediment samples, U-Pb zircon and apatite age data and apatite FT and

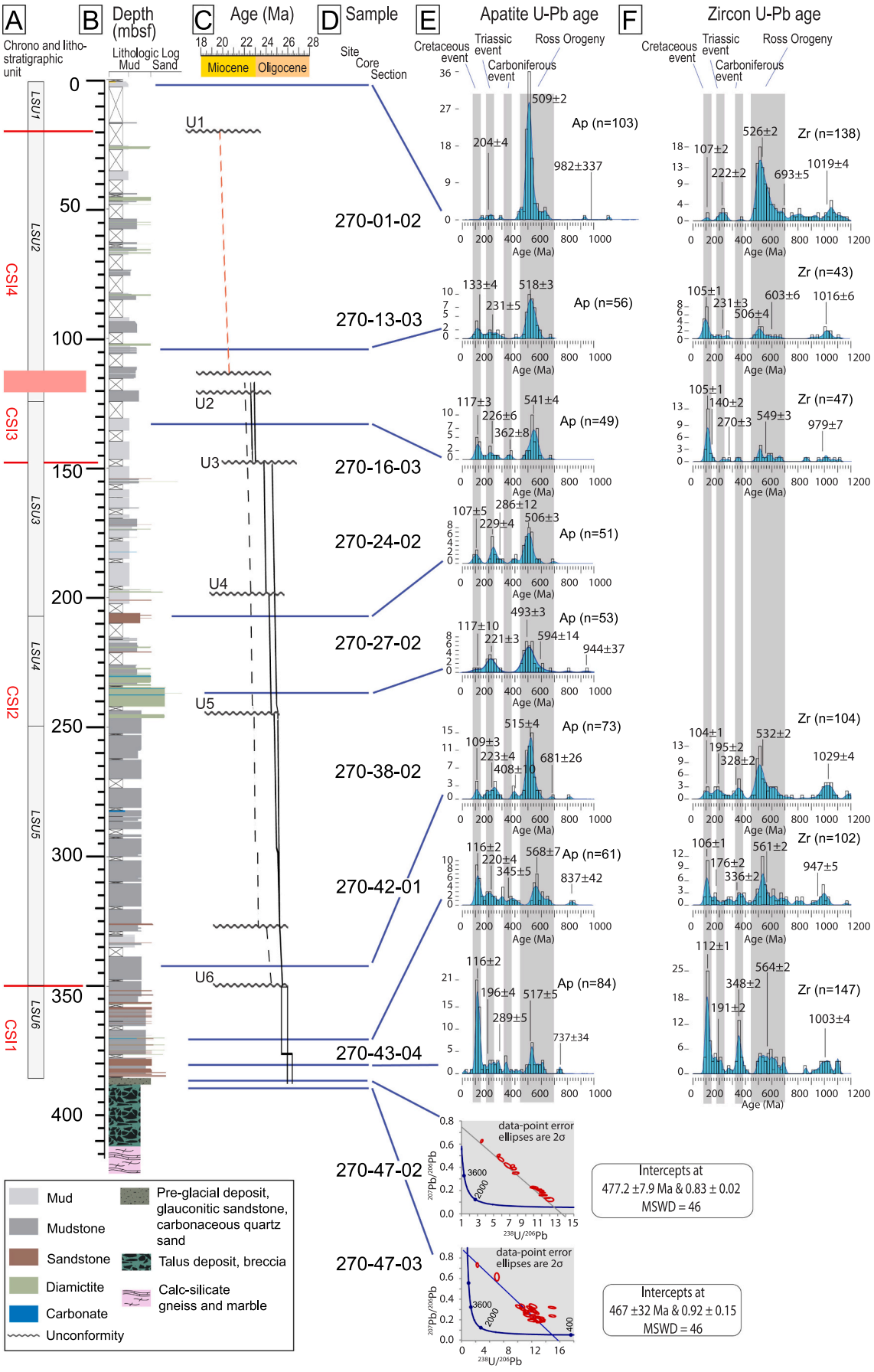

(caption on next page)

Fig. 2. DSDP Site 270 drill core and detrital apatite and zircon U-Pb age distributions. (A) Lithostratigraphic units (LSU) after Kraus (2016) and chronostratigraphic intervals (CSIs) modified from Kulhanek et al. (2019). (B) Drill core log. (C) Age model and main unconformities (U) are modified from Kulhanek et al. (2019). (D) Sample ID and stratigraphic position. (E) Apatite U-Pb diagrams; U-Pb ages are shown as Tera-Wasserburg plots for basement samples and as Kernel density estimation (KDE) plots for detrital samples. For the latter the grey age bars correspond qualitatively to tectonic events associated with the Ross Orogeny, Devonian-Carboniferous, Triassic and Cretaceous. (F) Zircon U-Pb diagrams; U-Pb ages are shown as Kernel density estimation (KDE) plots. Age bars (in grey) correspond qualitatively to events in the Ross Orogeny, Devonian-Carboniferous, Triassic and Cretaceous.

trace element data were acquired. For the two basement rocks and two samples from the diamictite strata, only apatite U-Pb age and trace element data were obtained (Fig. 2). U-Pb grain age distributions were analyzed with the Density Plotter software (Vermeesch, 2013) that undertakes Kernel Density Estimation (KDE), and determines the number of populations and its central age. Populations with less than three grains are not considered significant.

All the data produced, supporting the results and discussion, are free to download from the data set described in (Olivetti et al., 2023).

5.1. Apatite U-Pb dating

538 detrital and 41 basement apatites were analyzed (Fig. 2). The basement gneiss sample (a calc-silicate gneiss, 270–47-03) yields an unanchored Tera-Wasserburg lower intercept age of 467 ± 32 Ma, with a $^{207}Pb/^{206}Pb$ initial value of 0.92 ± 0.15, but with significant dispersion (MSWD = 46). In contrast, sample 270–47-02 (a composite sample from several clasts) from the breccia that overlies the basement rocks and is comprised mainly of leucogranite clasts yields an unanchored Tera-Wasserburg lower intercept age of 477.2 ± 7.9 Ma, with a $^{207}Pb/^{206}Pb$ initial value of 0.8318 ± 0.022 with a significantly lower MSWD (1.8). Both ages are consistent with involvement in the Ross Orogeny.

Detrital apatites from the Oligocene-Miocene strata yield U-Pb ages between c. 90 Ma and c. 700 Ma. The U-Pb apatite age distribution of the basal detrital samples 270–43-04 and 270–42-01 share some common features, consistent with them belonging to the same lithostratigraphic unit (LSU6 of Kraus, 2016) and chronostratigraphic unit CS1 (Kulhanek et al., 2019).

The oldest clastic sediment sample (270–43-04) is largely dominated by apatites with Cretaceous U-Pb ages (peak at c. 116 Ma) accompanied by a smaller Ross Orogeny peak (450 to 640 Ma), with a spread in ages between 200 and 380 Ma. Sample 270–42-01 yields similar peaks associated with Cretaceous magmatism and the Ross Orogeny, with a minor population from 220 to 345 Ma. In sample 270–38-02 there is a significant decrease in the Cretaceous population (109 Ma) and an increase in the Ross Orogeny peak. This pattern continues into samples 270–27-02 and 270–24-02 with the Cretaceous peak (117 Ma) decreasing in abundance and a Triassic population becoming the second most significant peak. The U-Pb apatite age peak corresponding to the Ross Orogeny represents the most abundant population. Samples 270–16-03 and 270–13-03 share common features, with the Cretaceous population representing the second most significant component after the dominant Ross Orogeny U-Pb age peak. The Triassic population is represented by only a few grains that cluster around 230 Ma while a small number of grains in sample 270–16-03 yield a Devonian age. Sample 270–01-02 (of Quaternary age) is completely different with respect to all other samples. The Cretaceous population is absent, the Triassic U-Pb age peak is very minor and Ross Orogeny detritus represents by far the most abundant U-Pb apatite age population.

5.2. Detrital zircon U-Pb age dating

642 zircons were analyzed from six detrital samples all of which have corresponding apatite U-Pb data (Fig. 2). The KDEs yield Late Neoproterozoic to Cretaceous U-Pb zircon age populations. The Ross Orogeny population is the most abundant in two samples (270–38-02, 270–01-02), the Cretaceous population is the most abundant in three samples (270–43-04, 270–16-03, 270–13-03) while in one sample the two U-Pb zircon populations are comparable (270–42-01). Grain age spectra are similar to the apatite U-Pb data, with only some small differences. These differences include a smaller peak associated with the Ross Orogeny in two samples (270–13-03 and 270–16-03). In all detrital zircon samples, an old (c. 1000 Ma) zircon population is detected, which is either absent or very minor in the corresponding detrital apatite U-Pb dataset.

5.3. Apatite trace element analysis

Trace element analysis of apatites from the basal calc-silicate gneiss (sample 270-43R-04 W, Tera-Wasserburg lower intercept age of 467 ± 32 Ma) shows an affinity with I-type granitoids and mafic rocks (IM group, Fig. 3). This implies that the trace element signature of apatite from medium/high-grade calc-silicates (a volumetrically minor rock type in the crust) are similar to those of IM mafic rocks and I-type granitoids, but no apatite from calc-silicates is incorporated in the literature database of O'Sullivan et al. (2020). In the granite talus clasts (sample 270–47-02), trace element analysis suggests an affinity with S-type and felsic I-type granitoids (S) and high-grade metamorphic rocks (HM), consistent with petrological analysis (Ford and Barrett, 1975), likely reflecting derivation from a high-grade metasedimentary rock which underwent anatexis.

Geochemical analysis of detrital apatites shows a trace element composition with very similar features in all the samples. The Cretaceous apatite population shows mainly an igneous affinity (primarily with I-type granitoids and mafic rocks = IM group) with a subordinate metamorphic rock affinity. The Ross Orogeny grain population is the only population consistently showing a significant proportion of apatite grains with a low-grade metamorphic affinity, consistent with regional metamorphism associated with the growth by plate-margin accretion (Goodge, 2020).

5.4. Apatite FT age distributions

Apatite FT dating was undertaken on six clastic sedimentary samples. The apatite FT single grain ages range between 21 and 439 Ma (Fig. 4). The single-grain FT ages were statistically decomposed into populations using DensityPlotter (Vermeesch, 2012) and the FT age distributions of the six samples are shown on Fig. 4b,c. In general, for the Miocene-Oligocene samples, the main AFT age population ranges between 69 Ma and 105 Ma (corresponding to between 46% and 57% of all grains) with an older population around 150–200 Ma. In samples 270–38-02, 270–16-03 and 270–13-03 a minor Cenozoic peak is also present. The Quaternary sample 270–01-02 presents a more varied distribution with four peaks at ca. 36 Ma, 70 Ma, 120 Ma and 180 Ma.

In Fig. 4c, apatite U-Pb age is plotted against FT age to i) detect apatite of volcanic origin. A volcanic origin can be proposed when the age from the high-temperature system (U–Pb) matches the cooling age through ~100 °C isotherm (AFT), representing rapid magmatic cooling, - and ii) to observe if apatite with different U-Pb age populations (likely indicating different source areas) experienced different exhumation episodes.

Such an approach can help to discriminate between different potential source areas. The comparison between apatite FT and U-Pb ages allow us to make several observations: (1) with the exception of sample 270–43-04, the AFT ages are younger than the U-Pb age and therefore

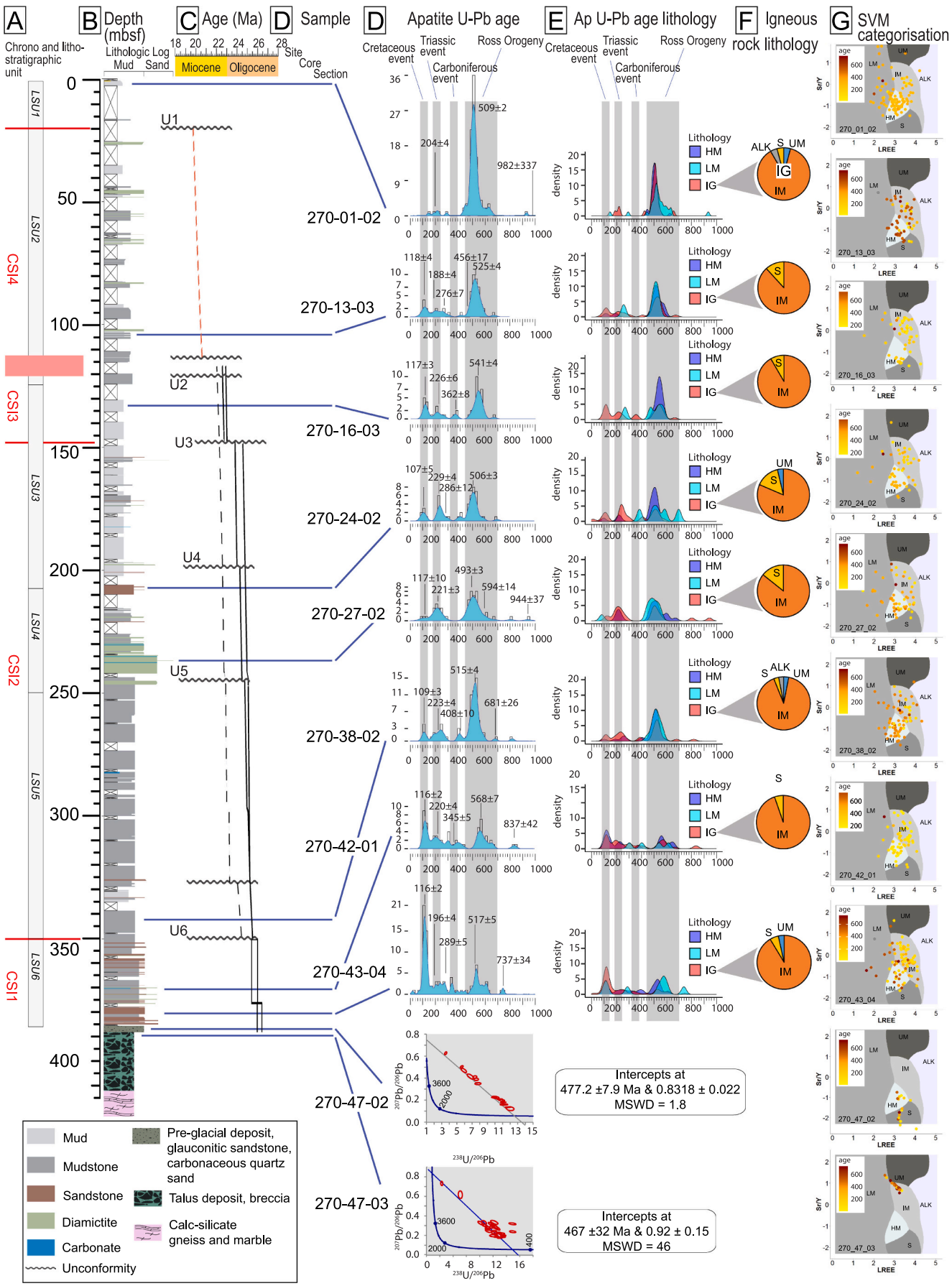

(caption on next page)

Fig. 3. DSDP Site 270 drill core, apatite U-Pb age and affinity with lithology source. (A) Lithostratigraphic units (LSU) after Kraus (2016) and chronostratigraphic intervals (CSIs) modified from Kulhanek et al. (2019). (B) Drill core log. (C) Age model and main unconformities (U) modified from Kulhanek et al. (2019). (D) Apatite U-Pb KDEs. (E) KDE plot of apatite U-Pb age divided into lithologies defined by the Support Vector Machine (SVM) categorization of O'Sullivan et al. (2020). HM – High-grade metamorphic apatite; LM - Low-grade metamorphic apatite; IG - igneous apatite that is a combination of the S, ALK, IM, and UM categories defined below. (F) Proportion of the S, ALK, IM, and UM categories within the IG group. (F) detrital apatites coloured by age compared to the SVM machine categorization based on a Sr/Y vs ΣLREE plot. Abbreviations for groups: ALK = alkali-rich igneous apatite; IM = mafic I-type granitoids and mafic igneous apatite; LM = low- and medium-grade metamorphic and metasomatic apatite; HM = partial-melts/leucosomes/high-grade metamorphic apatite; S=S-type granitoids and high aluminium saturation index (ASI) 'felsic' I-type apatite; UM = apatite from ultramafic rocks including carbonatites, lherzolites and pyroxenites.

volcanic apatite is a negligible component; (2) Cenozoic volcanic apatite is completely absent; (3) in several samples a < 45 Ma AFT population with Ross Orogeny U-Pb ages is present; (4) for sample 270–43-04, with not so distant AFT (ca. 80 Ma) and U-Pb ages (ca. 100 Ma), indicates a rapidly exhuming source area.

5.5. Clast petrology and distribution

A total of 3099 gravel-size clasts were identified in the DSDP Site 270 core (see Fig. 5).

The clasts are dominated by grey to very dark metamorphic lithics (73%) that are identified using optical microscopy as meta-sandstone and meta-siltstone, with a poorly developed schistosity.

Intrusive rocks form the second most abundant group (18%); they are usually grey to pink, medium grained, non-foliated granite to granodiorite. Clasts of mafic intrusive/dolerite are also present but very minor (1%). Volcanic rocks are poorly represented in the core (< 1%) with a few olivine-bearing basalt and trachytic clasts recognized. Felsic sub-volcanic rocks (2%) including rhyolitic porphyry, and sedimentary lithics (sandstone and mudstone, 2%) are also present.

The relative clast type abundances typically do not show any significant variations along the core (Fig. 5). Felsic porphyry becomes more abundant below c. 200 mbsf (CSI 1 and CSI 2). Dolerite/mafic intrusive clasts are absent in the Miocene portion of the core below c. 150 mbsf (CSI 1 and CSI 2).

5.6. Multidimensional scaling

To visualize the provenance similarities between the samples, a multidimensional scaling (MDS) map (Fig. 6) is employed. The MDS map was calculated using the Kolmogorov-Smirnov statistic (Vermeesch, 2013) where the distance between the samples reflects the similarity/dissimilarity in age distributions. The MDS map (Fig. 6a) for apatite U-Pb ages mimics, in general, the separation in chronostratigraphic interval (Kulhanek et al., 2019) and lithostratigraphic units revised by Kraus (2016): sample 270–43-04 and 270–42-01 plot close to each other and they belong to the basal unit (LSU6); samples 270–24-02 and 270–27-02 also plot close together and are part of the same unit LSU4; sample 270–01-02 from the Quaternary sediments plots to the far right of the diagram, far away from the other samples. To compare the zircon and apatite U-Pb ages we produced a MDS map (Fig. 6b) for ages younger than 800 Ma, to reduce the influence of the old (c. 1 Ga) zircon population which is absent in the apatite U-Pb spectra. The map shows that in four samples (270–43-04, 270–42-01, 270–38-02 and 270–01-02), the apatite and zircon data plot close to each other, suggesting that in most cases, the age distribution employing different minerals shows large similarities.

6. Discussion

6.1. Potential source regions and regional provenance trends

The U-Pb ages of the detrital apatite and zircon grains range from c. 100 to c. 1000 Ma, with four populations that are found in both the apatite and zircon spectra: i) a Cretaceous population (c. 100 Ma), ii) a Triassic population (c. 200 Ma), iii) a Carboniferous-Devonian population (340–370 Ma) and iv) a Ross Orogeny age population (Cambrian to Latest Neoproterozoic, 480 to 600 Ma).

These four populations are identified in all previous single-grain provenance studies in the Ross Sea region which have mainly focused on Last Glacial Maximum (LGM, Licht et al., 2014; Perotti et al., 2017) samples and, only very recently, on Miocene stratigraphic intervals (Marschalek et al., 2021). We compare the detrital spectra detected in DSDP Site 270 with the provenance patterns proposed for the Miocene, LGM and Holocene sediments to evaluate changes in topography and glacial erosional style. There is limited data on apatite and zircon fertility in Antarctic basement rocks, and caution should therefore be taken, particularly when comparing the relative abundance of different age populations.

The source for Cretaceous apatite in Quaternary sediments of the Ross Sea is usually proposed as the intrusives and high-grade metamorphic rocks (Byrd Coast Granite and migmatitic domes) associated with the Cretaceous magmatic arc and its associated back-arc extension (Licht et al., 2014, Siddoway, 2008, 2021, Pankhurst et al., 1998; Jordan et al., 2020). Derivation from calc-alkaline granites and migmatites is also supported by the apatite trace-element analysis (Fig. 3e, f, g), which shows that apatites of this age have an affinity with I-type granitoids and mafic rocks and high-grade metamorphic rocks. The Byrd Coast Granite and migmatitic domes are presently exposed in the eastern MBL (Fig. 1), and it is possible that large portions of the WA crust are formed of similar rocks.

The provenance of the Triassic grains is uncertain because outcrops of magmatic and metamorphic rocks of this age are very limited. Triassic detrital zircons have been found in LGM sediments of the eastern Ross Sea and also from the Siple Coast Ice streams (Licht et al., 2014, Perotti et al., 2017). Triassic zircons have also been detected in Miocene sediments drilled in the central Ross Sea from stratigraphic intervals interpreted to have been sourced from WA (Marschalek et al., 2021). Moreover, Triassic detrital zircons have been found within Triassic sandstones of the Beacon Supergroup and are interpreted as derived from a volcanic arc (Elliot et al., 2017, 2019). Outcrops of Triassic magmatic rocks related to the Gondwanide Orogeny are sparsely exposed along the coast of western MBL, Thurston Island and the Antarctic Peninsula, but these possible source areas are too far away to be plausible sources for sediments in the DSDP Site 270 site and the Ross Embayment. It is possible that rocks of similar age are found in the southernmost WARS (Fig. 1), a region that is a source area for ice moving from southern WA within the Ross Embayment. If so, this inferred prolongation of the Gondwanide Orogeny rocks in the Ross Sea sector must have been exposed to the surface by Oligocene times. All Triassic grains in the samples from DSDP Site 270 show AFT ages much younger than their apatite U-Pb ages (Fig. 4c), thus implying a source from exhumed bedrock rather than a volcanic origin, unlike the Triassic volcanic populations within the Beacon Supergroup sediments (Elliot et al., 2017, 2019; Paulsen et al., 2017).

The Devonian-Carboniferous population is a very minor population that is only clearly present in samples 270–43-04, 270–42-01, 270–38-02 and 270–16-03. The Ford Granodiorite of the MBL is a potential source region for these grains as well as other rocks in the region involved in the Lachlan Orogeny.

The Ross Orogeny grains can potentially be derived from two sources: i) first-cycle sourcing from the Granite Harbour Intrusive Complex that crops out in the TAM, or ii) recycling from Paleozoic metaturbidites that crop out both in WA (Swanson Fm) and in the TAM (Byrd and

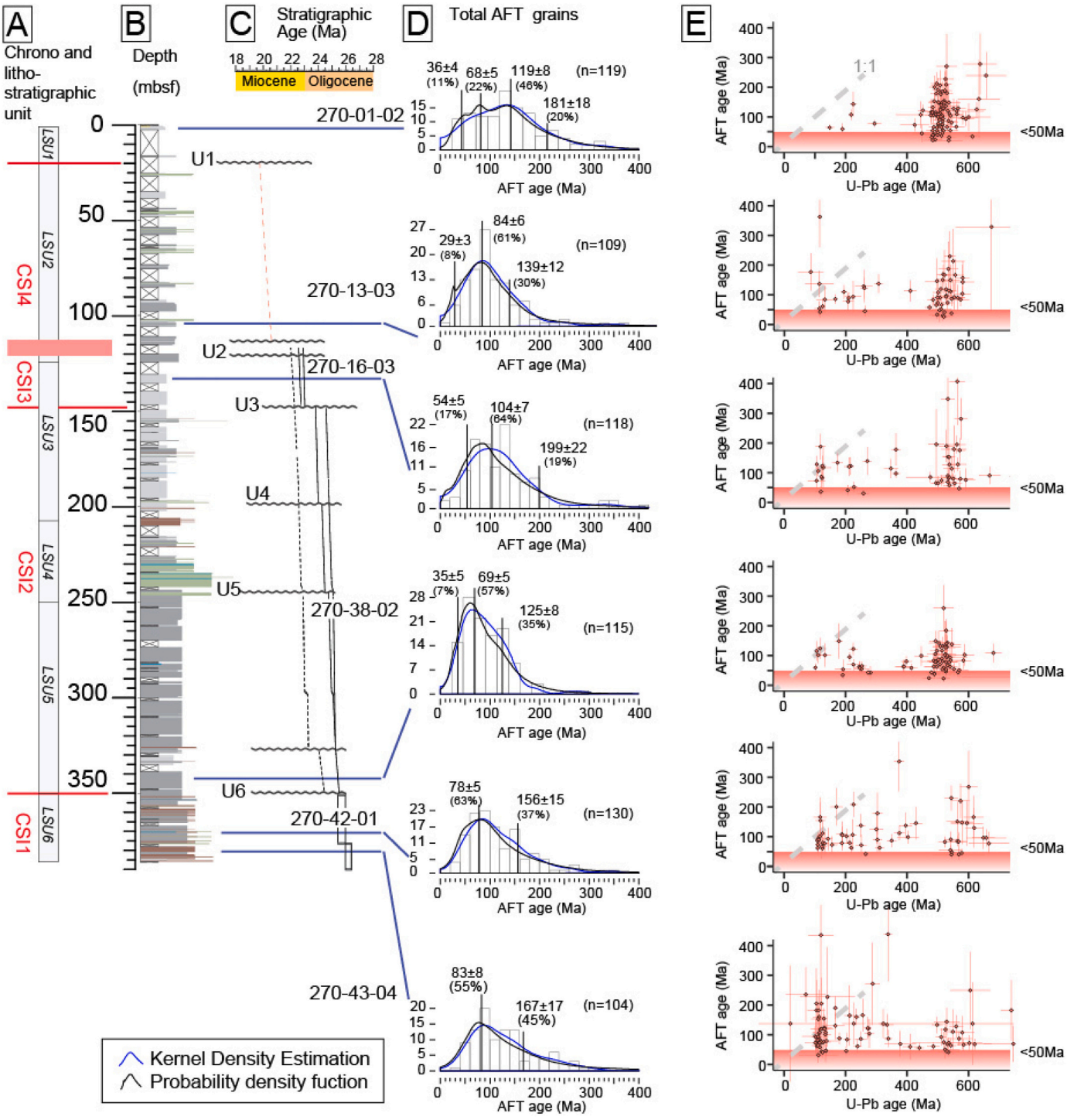

Fig. 4. Apatite fission-track (AFT) age results: (A) Lithostratigraphic units (LSU) after Kraus (2016) and chronostratigraphic intervals (CSIs) modified from Kulhanek et al. (2019). (B) Drill core log. (C) age model modified from Kulhanek et al. (2019). (C) Histograms and KDE plots of the AFT age distributions with the age of the populations shown. KDEs generated using the density plotter software (Vermeesch, 2012). (D) AFT vs U-Pb age. The dashed grey line represents grains with the same AFT and U-Pb age that indicates a rapid cooling from ca. 400–500 °C to ca. 100 °C, suggesting either a volcanic origin or very rapid exhumation. The red band indicates AFT ages <50 Ma, likely sourced from the TAM. (For interpretation of the references to colour in this figure legend, the reader is referred to the web version of this article.)

Robertson Bay groups). Therefore, the Ross Orogeny population is not diagnostic of a specific provenance. The Ross Orogeny rocks exposed along the TAM are represented mainly by late orogenic intrusives (470 to 530 Ma) (Goodge, 2020 and reference therein), while detrital zircon grains in turbidites, in general yield slightly older ages (Estrada et al., 2016), likely because they were fed by early orogenic detritus from metamorphic and magmatic rocks. The trace element composition of detrital apatite in this study is consistent with this interpretation, as it indicates that older Ross Orogeny apatites have a metamorphic affinity while younger Ross Orogeny apatites show an affinity with granitoid rocks (Fig. 3). The oldest detritus correspond to Grenvillian U-Pb zircon ages, which are not recorded in the apatite U-Pb spectra. It is likely that

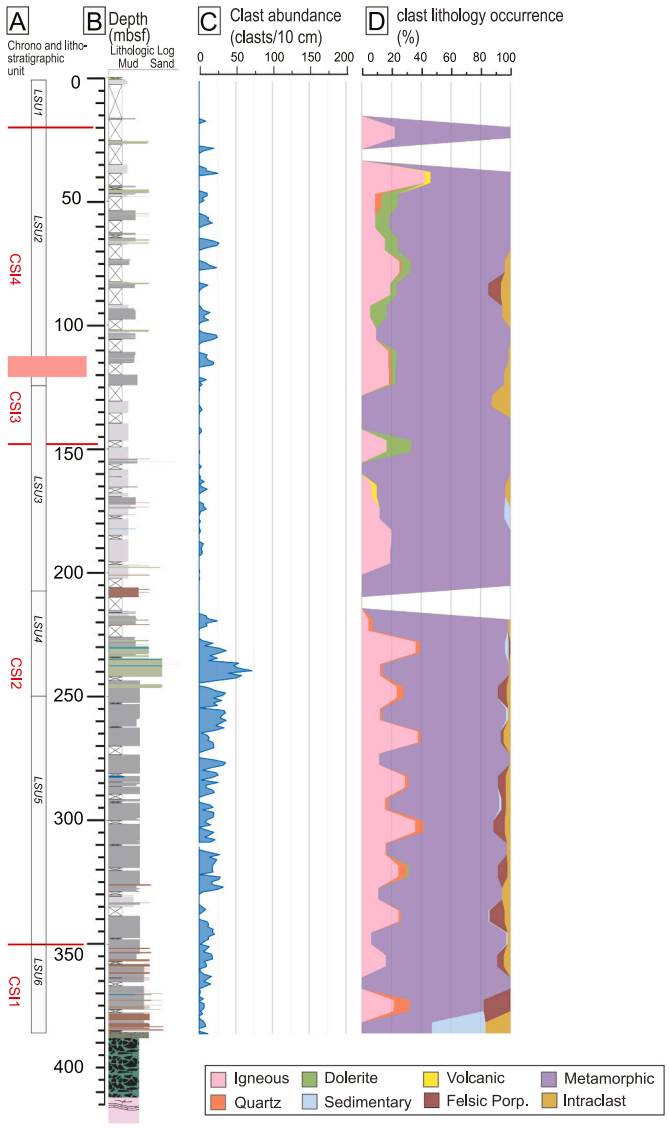

Fig. 5. (A) Lithostratigraphic units (LSU) after Kraus (2016) and chronostratigraphic intervals (CSI) modified from Kulhanek et al. (2019). (B) Drill core log. (C) Clast abundance. (D) Percentages of different clast lithologies.

any Grenvillian apatite either was recrystallized or age reset during the Ross Orogeny.

6.2. *Geographic provenance and implications for the climatic and tectonic evolution*

6.2.1. *Age of the basement and talus*

The apatite Tera-Wasserburg lower intercept age of 467 ± 32 Ma from the calc-silicate gneiss yields a late Ross Orogeny age, albeit with significant dispersion. Ford and Barrett (1975) correlate these rocks with metasedimentary rocks of the Skelton Group in southern Victoria Land (TAM) which are believed to record a long and multiphase metamorphic evolution from the Latest Neoproterozoic to Ordovician, as shown by monazite ages ranging from c. 600–500 Ma (Hagen-Peter and Cottle, 2016; Goodge, 2020). A titanite U-Pb age of 437 ± 6 Ma was reported by Mortimer et al. (2011) from the same basal gneiss that they associated with Lachlan deformation. We envisage that the apatite in the calc-silicate gneiss forming the basement in the DSDP Site 270 core crystallized during Ross Orogeny but was partially recrystallized (or age reset) during the younger Lachlan deformation phase.

The overlying sequence with granitic clasts, has been interpreted as a

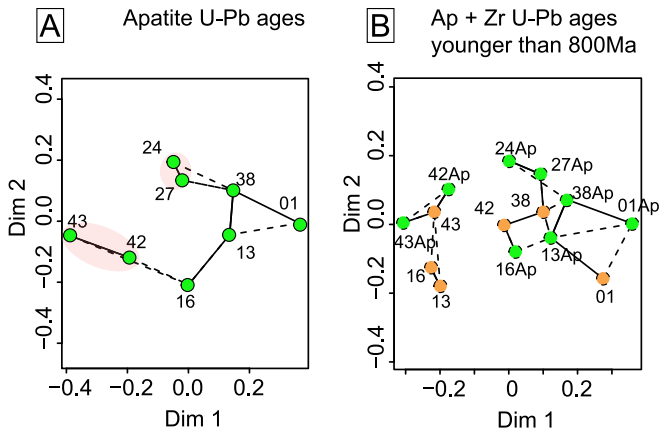

Fig. 6. Multidimensional scaling (MDS) map calculated using the Kolmogorov-Smirnov statistic. The map shows relative statistical similarities between samples. Solid lines mark the closest neighbours and dashed lines the second closest neighbours. Green and orange circles represent apatite and zircon U-Pb ages respectively. (A) MDS plot of apatite U-Pb age distributions. The pink circles represent samples from the same lithostratigraphic units (after Kraus, 2016) (B) MDS plot of apatite and zircon for U-Pb ages younger than 800 Ma. (For interpretation of the references to colour in this figure legend, the reader is referred to the web version of this article.)

talus deposit and therefore would represent a very local provenance (Ford and Barrett, 1975). It yields a Tera-Wasserburg lower intercept age of 477.2 ± 7.9 Ma, similar to the age of the Ross Orogeny intrusives, especially in southern Victoria Land (Cox et al., 2000). It is noteworthy that rocks associated with the Ross Orogeny are extremely rare in the crystalline basement of MBL; this age for the granite clasts in the talus breccia suggests that the Central High basement has a closer affinity to the basement of the TAM.

6.2.2. *Basal unit (CSI1 ~ 26.4 to ~25.4 Ma)*

The provenance of samples 270–43-04 and 270–42-01 has major implications on the tectonic evolution and exhumation of the Central High crust and the regional sediment routing systems. The two samples show a prominent Cretaceous zircon and apatite U-Pb age peak that is also characteristic of Quaternary sediments in the Ross Sea region. In the Ross Sea, a Cretaceous peak in single-grain detrital age spectra is considered characteristic of provenance from WA (Licht et al., 2014; Perotti et al., 2017) and such ages have not been detected in the underlying basement rocks of the DSDP 270 sediments. The basal unit (LSU6, corresponding to CSI 1) has recently been interpreted as a glaciomarine turbidite sequence deposited in close proximity to a terrestrial margin and the front of an ice cap (Kraus, 2016) likely located to the west or southwest of the DSDP 270 site, in agreement with seismic interpretations (De Santis et al., 1995).

Hence although a Cretaceous detrital population is often considered to represent a MBL provenance (e.g. Licht et al., 2014; Marschalek et al., 2021 for the LGM and Miocene), we infer a local provenance from the Central High (Fig. 7h). A MBL provenance would imply that the Eastern Basin was shallow enough to allow turbidity currents to be transported from the coast of MBL, but this is not supported by paleotopographical (see Paxman et al., 2019) and seismic stratigraphy data (De Santis et al., 1995, 1999).

The provenance of the glacial sediments 270–43-04 and 270–42-01 from local ice caps located on the emerged portion of the Central High concurs with the reconstructed Oligocene topography and ice volumes, which show a small ice cap over the MBL and CH (Jamieson et al., 2010; Paxman et al., 2019; Naish et al., 2022). The existence of large areas still lying above sea level, until ca. 26 Ma, in the Ross Sea was inferred by De Santis et al. (1995) and Brancolini et al. (1995).

Because the basal LSU6 unit is sourced locally, the high abundance of

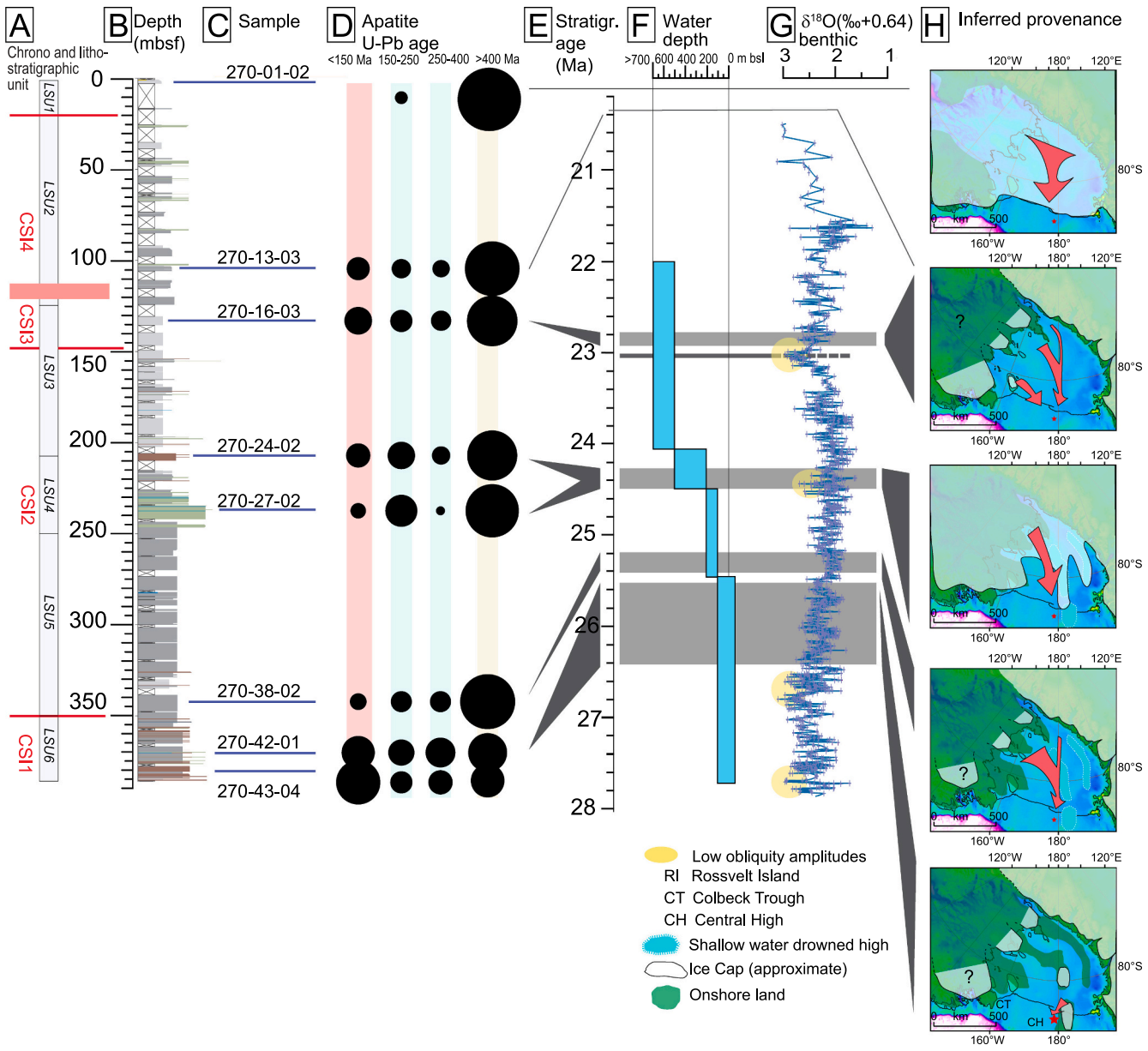

Fig. 7. Comparison between core stratigraphy, apatite U-Pb age populations and the paleoclimatic record. The ice cap limit is meant to visualize the variation of the ice front and not the exact location of the inferred ice cap. (A) Lithostratigraphic units (LSU) are after Kraus (2016) and chronostratigraphic intervals (CSI) are modified from Kulhanek et al. (2019). (B) Drill core log. (C) Sample ID and stratigraphic position. (D) Relative proportions of the four apatite U-Pb age populations for each sample. (E) Stratigraphic age. (F) Basin subsidence (curve from Naish et al., 2022). (G) $\delta^{18}O$ curve for the Oligocene with yellow ellipses that mark maximum $\delta^{18}O$ during low obliquity amplitudes from Pälike et al., 2006. (H) inferred provenance directions and ice volume changes with time. (For interpretation of the references to colour in this figure legend, the reader is referred to the web version of this article.)

Cretaceous grains implies involvement of the Central High rocks in a Cretaceous magmatic and high-grade metamorphic event, similar to MBL. Moreover, the cooling and exhumation history recorded by the detrital AFT ages suggests that source area of the Cretaceous detritus cooled rapidly from 100 Ma and 80 Ma, probably following rapid exhumation linked to detachment faulting (Fitzgerald and Baldwin, 1997). The detrital AFT ages in samples 270–43-04 and 270–42-01 are very consistent with the AFT ages obtained from the basement gneiss in DSDP Site 270 (Fitzgerald and Baldwin, 1997), the AFT age of Cretaceous mylonites in the Colbeck trough (Siddoway et al., 2004) and AFT ages from MBL (Zundel et al., 2019), highlighting widespread exhumation associated with Cretaceous crustal extension.

An affinity of the Central High crust with MBL has been proposed based on geophysical data (Siddoway, 2008), while slightly less dense crust and the presence of a magnetic anomaly below the DSDP site 270 (Tinto et al., 2019) suggest the Central High rocks have an affinity with East Antarctic crust. In this scenario, the rocks of the Central High represent a mixed domain formed of gneisses (similar to rocks of Skelton Group, TAM) and intruded by plutons associated with the Ross Orogeny (age of the granitic clasts in the talus deposit) that locally experienced Cretaceous high-grade metamorphism and magmatism. Central High thus represents the boundary between WA and TAM (and EA) crust, as proposed by Tinto et al. (2019).

6.2.3. *Late Oligocene – (base of CSI 2– 25.5 – ~24.4 Ma)*

The sediments corresponding to CSI 2 were deposited in an open marine environment, with deeper water depths than the underlying units (Leckie and Webb, 1983). Deposition of IRD is significant in this

unit (LSU5 of Kraus, 2016; base of CSI 2 of Kulhanek et al., 2019). The change in apatite U-Pb and AFT age distributions in sample 270–38-02 relative to the units below (270–43-04 and 270–42-01, LSU6 of Kraus, 2016) suggests a different provenance than the proximal Central High. The Central High was likely almost already drowned during LSU5 deposition because of ongoing subsidence (De Santis et al., 1995; Paxman et al., 2019; Naish et al., 2022) and thus was no longer a prominent source of sediments, and hence any Cretaceous peak detected in LSU5 and in younger strata was likely derived from WA, which is considered the most likely source during the Miocene and LGM (Licht et al., 2014; Perotti et al., 2017; Marschalek et al., 2021). Sediment supply from WA through IRD suggests the presence of an onshore ice sheet whose marine extent is difficult to constrain (Fig. 7h). The scarcity of dolerite clasts in the clast dataset similar to the other Miocene samples in the core below c. 150 mbsf (Fig. 5), also implies a major contribution from an ice center located in WA (Fig. 7h) as dolerite is a lithology usually associated with the Jurassic Ferrar Group in the TAM.

In sample 270–38-02, a Cenozoic peak appears for the first time in the AFT age distribution (c. 35 Ma)(Fig. 4b). Eight grains comprising this AFT Cenozoic peak yield U-Pb ages characteristic of the Ross Orogeny (Fig. 4c). They are interpreted as representing a minor component of TAM detritus because: i) at the time of deposition of sample 270–38-02, the TAM were already actively exhuming (Fitzgerald, 1992); ii) the TAM were already a source of AFT grains younger than 70 Ma in the marine record (Olivetti et al., 2013), and iii) no evidence of denudation between 45 Ma and 26 Ma has been found in the MBL (Zundel et al., 2019). Additionally, at this time the morpho-structural highs between the TAM and the Eastern Basin were subsiding (see Paxman et al., 2019), and were likely no longer obstacles to sediment transport into the Eastern Basin. But the amount of TAM-sourced detritus is likely minor given that dolerite clasts are absent. The relative decrease, with respect to the lower samples, in Cretaceous U-Pb ages and the increase in the Triassic U-Pb ages implies a source located in the southern TAM, close to the boundary between MBL and southern TAM (Fig. 7h). Sample 270–38-02 therefore implies a distal glacial source and sedimentation in an open marine environment, that is consistent with a progressive deepening due to sea floor subsidence (Naish et al., 2022; Duncan et al., 2022)(Fig. 7).

6.2.4. *Latest Oligocene (CSI2 ~ 25.5 – ~24.4 Ma)*

Unit LSU4 (samples 270–27-02 and 270–24-02) shows sedimentological characteristics of a diamictite deposited in a range of glaciomarine environments proximal to an ice sheet front, and yields the clearest sedimentological evidence for a diamictite deposit in the entire drill core (Leckie and Webb, 1983; Kraus, 2016). The apatite U-Pb age distribution is substantially different from all other samples (Figs. 2, 3), primarily because of the scarcity of Cretaceous grains and the well-developed Triassic population. This Triassic population rarely occurs in sediments in the Ross Sea region. However it is present in Quaternary sample 94–63 (Eastern Basin), in the Bindschadler Ice Stream (BIS, Fig. 1) tills (Licht et al., 2014) and in sequence 2 of IODP Site U1521, considered as evidence of a WA provenance transported by a substantial ice sheet over the Ross Sea continental shelf (Marschalek et al., 2021).

A local provenance from the Central High is considered very unlikely, because it implies a very southern (present-day coordinates) extension of the Gondwanide deformational domain (Triassic orogeny), that has never been documented or even considered in the literature (Elliot, 2013; Elliot et al., 2017, 2019; Paulsen et al., 2017). Triassic crystalline bedrock is presently sparsely exposed, cropping out in western MBL, Thurston Island and Antarctic Peninsula, and even if the Triassic magmatism had a more widespread distribution than the present-day outcrops, we believe that the Central High is located too far away from the inferred subduction zone and active margin to be the location of a magmatic arc. We suggest, in agreement with Marschalek et al. (2021), therefore that the Triassic source was located somewhere in southern WA (Fig. 7h). The Triassic peak is usually associated with the occurrence of felsic porphyries in the clast assemblage (Fig. S1); its source is unknown. This observation may suggest the presence of a Permo-Triassic belt beneath the southern WARS.

Based on the provenance data and the sedimentological evidence for deposition proximal to an ice sheet margin, we hypothesize that a substantial ice sheet advanced sufficiently far to transport detritus from the southern WARS into the Ross Embayment proximal to the drill location (Fig. 7h). In support of this scenario, we note that Ross Sea floor was shallower than today, and topographic modeling indicates that large parts of the WARS (especially the southernmost portion) were emerged (Wilson et al., 2012; Paxman et al., 2019), thus more easily sustaining a continental ice sheet flowing from southern West Antarctica.

Recent sea surface temperature estimates show cooling of ~3 °C at 24.5 Ma in the Ross Sea regions (Duncan et al., 2022). These data are in agreement with recent topography-ice volume reconstructions (Pollard and DeConto, 2020), supporting the hypothesis of a short-lived marine-based WAIS advance into the Ross Sea at 24.5 Ma (Duncan et al., 2022), even though this is a time period characterized by a long-term global-scale decrease in $\delta^{18}O$ values (Pälike et al., 2006; Duncan et al., 2022). Neverthless, it is interesting to note that the deposition of the diamictite matchs a local maximum in the $\delta^{18}O$ value in the marine record of ODP Site 1218 that is synchronous with a period of low obliquity amplitude (Fig. 7g), an astronomical configuration that favors the development of ice sheets (Levy et al., 2019).

Therefore, data presented in this study highlights a source region located in the southern WARS, suggesting a WAIS expansion in the Oligocene thus predating the recently recognized oldest phase of WAIS expansion dated at 17.5 to 17.7 Ma by Marschalek et al. (2021).

6.2.5. *Latest Oligocene – Early Miocene (CSI 3 and CSI 4– 25.5 to ~20 Ma)*

Samples 270–13-03 and 270–16-03 are from two distinct lithostratigraphic units (Kraus, 2016) and chronostratigraphic intervals separated by ~2.5 myr (Kulhanek et al., 2019). Nevertheless, they show similar apatite and zircon U-Pb age spectra, suggesting very similar provenance and sediment routing systems. Sample 270–16-03 was collected from LSU3, deposited during a period of high sea level in an ice-distal setting (Kulhanek et al., 2019). Although LSU2 (from which sample 270–13-03 was collected) shows evidence of a renewed intensification of glacial conditions, the environment of deposition is interpreted as ice-distal and deep marine (Leckie and Webb, 1983). The Cretaceous and Carboniferous-Devonian populations are consistent with a MBL source of these sediments, also supported by the presence of Triassic grains whose provenance is inferred to be from southern WA (Fig. 7h). These U-Pb age distributions are consistent with open marine environment conditions (Fig. 7h), whereby the grains have a mixed source from WA with a possible contribution from the southern TAM as implied by the <50 Ma AFT age population.

It is important to note the MDS plots for samples 270–13-03 and 270–38-02. In the apatite U-Pb MDS they plot near each other suggesting a similar age distribution that could reflect a similar open marine environment. The differences in the zircon U-Pb age MDS could be due to a (minor) relative difference in the Ross age populations between the two samples. The stratigraphic age of sample 270–16-03 is slightly younger than 23 Ma and therefore post-dates the Mi-1 glacial event that is not preserved in the DSDP Site 270 record. Ice-distal sourcing is supported by a period of inferred deglaciation as suggested by geochemical proxies (Duncan et al., 2022; Naish et al., 2022).

6.2.6. *Quaternary*

Apatite and zircon U-Pb spectra of the youngest sample are radically different from all the other samples in the DSDP Site 270 drill core, as shown also by the MDS plot (Fig. 4). The age distribution of sample 270–01-02 shows some similarities with age-spectra of the Whillans and Kamb Ice Stream tills drilled in the region of the Siple Coast (Licht et al., 2014). These samples represent LGM tills flowing from the southern WARS into the Ross Ice Shelf. The similarity in age spectra suggests the

same provenance for this Quaternary sample which is consistent with LGM paleo-ice flow configuration (Licht et al., 2014; Perotti et al., 2017, 2018; Li et al., 2020) (Fig. 7h).

7. Conclusions

Using a multi-proxy single-grain provenance approach of zircon U-Pb dating and apatite U-Pb, fission track and trace element analyses on the same grains, coupled with petrology of gravel-sized clasts, we constrain the provenance of Oligocene-lower Miocene glaciomarine sediments to provide insights into the geological and climatic evolution of the Ross Sea region at the time.

In particular we propose that:

i) the basement of the Central High belongs to the East Antarctica crust: the calc-silicate basement gneiss in DSDP Site 270 yields a dispersed Tera-Wasserburg lower intercept U-Pb age of 467 ± 32 Ma, while the overlying granitic talus clasts yield an age of 477.2 ± 7.9 Ma. These ages are characteristic of the Ross Orogeny and imply that the Central High basement rocks have a close affinity to the crust of the TAM.

ii) the Central High crust was involved in Cretaceous rifting: a significant Cretaceous detrital U-Pb apatite and zircon age population is detected in two samples from the basal unit. Literature data (seismic profiles, sedimentological interpretations and paleotopography modeling) show that these basal deposits were sourced proximally.

iii) sediment provenance changes during the late Oligocene show that the Central High is already drowned: there is a marked provenance switch with the Cretaceous U-Pb age population decreasing and the Triassic age population increasing. The Triassic population, coupled with the Cretaceous and the Carboniferous-Devonian ones, are indicative of source regions located between the southern TAM and the MBL. Moreover, AFT analysis shows several grains with Ross Orogeny U-Pb ages and Cenozoic (<50 Ma) AFT ages, implying derivation from southern TAM basement.

iv) the uppermost Oligocene diamictite represents a major glacial episode of regional significance: two samples from glacial deposits interpreted as proximal to the ice-sheet front, show a detrital signature very different to all other samples (a major Triassic apatite U-Pb age population and a minor Cretaceous U-Pb age population). The Triassic U-Pb age peak suggests very distant sourcing, likely from southern West Antarctica. A large continental ice sheet is required to source detritus from southern West Antarctica to the DSDP Site 270 site in the Ross Sea. This diamictite was deposited synchronous with a c. 3 °C paleo-temperature drop in the Ross Sea. The sediment provenance signature indicates a reassessment of the paleo-ice flows, implying they are mainly from the southern WA, and strongly supports a major terrestrial ice advance of a WAIS in the Ross Sea during a glacial advance at 24.5 Ma.

CRediT authorship contribution statement

Valerio Olivetti: Conceptualization, Formal analysis, Data curation, Visualization, Funding acquisition, Writing – original draft. **Maria Laura Balestrieri:** Conceptualization, Formal analysis, Data curation, Funding acquisition, Writing – original draft. **David Chew:** Methodology, Formal analysis, Writing – review & editing. **Luca Zurli:** Investigation, Formal analysis, Writing – review & editing. **Massimiliano Zattin:** Validation, Writing – review & editing. **Donato Pace:** Investigation, Formal analysis. **Foteini Drakou:** Investigation, Formal analysis. **Gianluca Cornamusini:** Validation, Writing – review & editing. **Matteo Perotti:** Investigation, Formal analysis, Funding acquisition, Writing – review & editing.

Declaration of Competing Interest

The authors declare that they have no known competing financial interests or personal relationships that could have appeared to influence the work reported in this paper.

Data availability

Data are available in Olivetti et al., (2023) https://doi.org/10.5880/fidgeo.2022.040

Acknowledgements

This work is dedicated to Franco M. Talarico, who has been a good friend and constant source of inspiration for all of us. We thank Laura De Santis for helpful discussions. We are grateful to reviewers Kathy Licht, Peter Bijl and an anonymous reviewer for their very constructive comments. This work used archival Deep Sea Drilling Project (DSDP) samples provided by the International Ocean Discovery Program (IODP). The research was carried out with the financial support of the Italian Programma Nazionale di Ricerche in Antartide (Grant number PNRA18_00233). DC and FD acknowledge support from a research grant from Science Foundation Ireland (SFI) under grant number 13/RC/2092_P2 (iCRAG, the SFI Research Centre in Applied Geosciences). VO and MZ were supported also by Geosciences Department funding (BIRD_182501).

Appendix A. Supplementary data

https://doi.org/10.1016/j.gloplacha.2023.104042

References

Behrendt, J.C., 1999. Crustal and lithospheric structure of the West Antarctic Rift System from geophysical investigations — a review. Glob. Planet. Chang. 23, 25–44.
Bernet, M., Brandon, M.T., Garver, J.I., Molitor, B.R., 2004. Fundamentals of detrital zircon fission-track analysis for provenance and exhumation studies with examples from the European Alps. Geol. Soc. Am. Spec. Pap. 378, 25–36.
Brancolini, G., Cooper, A.K., Coren, F., 1995. Seismic facies and glacial history in the western Ross Sea (Antarctica). In: Geology and Seismic Stratigraphy of the Antarctic Margin, 68, pp. 209–233.
Brandon, M.T., Roden-Tice, M.K., Garver, J.I., 1998. Late Cenozoic exhumation of the Cascadia accretionary wedge in the Olympic Mountains, Northwest Washington State. Geol. Soc. Am. Bull. 110, 985–1009.
Burgess, S.D., Bowring, S.A., Fleming, T.H., Elliot, D.H., 2015. High-precision geochronology links the Ferrar large igneous province with early-Jurassic Ocean anoxia and biotic crisis. Earth Planet. Sci. Lett. 415, 90–99.
Cherniak, D.J., Watson, E.B., 2001. Pb diffusion in zircon. Chem. Geol. 172 (1–2), 5–24.
Chew, D.M., Spikings, R.A., 2021. Apatite U-Pb Thermochronology: A Review. Minerals 11 (10), 1095.
Chew, D.M., Sylvester, P.J., Tubrett, M.N., 2011. U-Pb and Th-Pb dating of apatite by LA-ICPMS. Chem. Geol. 280 (1–2), 200–216. https://doi.org/10.1016/j.chemgeo.2010.11.010.
Chew, D.M., Petrus, J.A., Kamber, B.S., 2014. U-Pb LA-ICPMS dating using accessory mineral standards with variable common Pb. Chem. Geol. 363, 185–199. https://doi.org/10.1016/j.chemgeo.2013.11.006.
Cox, S.C., Parkinson, D.L., Allibone, A.H., Cooper, A.F., 2000. Isotopic character of Cambro-Ordovician plutonism, southern Victoria Land, Antarctica. N. Z. J. Geol. Geophys. 43 (4), 501–520.
Davey, F.J., Brancolini, G., 1995. The Late Mesozoic and Cenozoic structural setting of the Ross Sea region. Geol. Seism. Stratigr. Antarct. Margin 68, 167–182.
De Santis, L., Anderson, J.B., Brancolini, G., Zayatz, I., 1995. Seismic record of late Oligocene through Miocene glaciation on the Central and Eastern Continental Shelf of the Ross Sea. In: Cooper, A.K., Barker, P.F., Brancolini, G. (Eds.), Antarctic Research Series (Volume 68): Geology and Seismic Stratigraphy of the Antarctic Margin. American Geophysical Union, Washington, DC, pp. 235–260.
De Santis, L., Prato, S., Brancolini, G., Lovo, M., Torelli, L., 1999. The Eastern Ross Sea continental shelf during the Cenozoic: implications for the West Antarctic ice sheet development. Glob. Planet. Chang. 23 (1–4), 173–196.
Di Vincenzo, G., Grande, A., Rossetti, F., 2014. Paleozoic siliciclastic rocks from northern Victoria Land (Antarctica): Provenance, timing of deformation, and implications for the Antarctica-Australia connection. GSA Bull. 126 (11–12), 1416–1438. https://doi.org/10.1029/AR068p0235.
Duncan, B., McKay, R., Levy, R., Naish, T., Prebble, J.G., Sangiorgi, F., Bendle, J., 2022. Climatic and tectonic drivers of late Oligocene Antarctic ice volume. Nat. Geosci. 15 (10), 819–825.
Elliot, D.H., 2013. The geological and tectonic evolution of the Transantarctic Mountains: a review. Geol. Soc. Lond., Spec. Publ. 381 (1), 7–35.
Elliot, D.H., Fanning, C.M., Hulett, S.R.W., 2015. Age provinces in the Antarctic craton: evidence from detrital zircons in Permian strata from the Beardmore Glacier region, Antarctica. Gondwana Res. 28, 152–164. https://doi.org/10.1016/j.gr.2014.03.013.

Elliot, D.H., Fanning, C.M., Isbell, J.L., Hulett, S.R., 2017. The Permo-Triassic Gondwana sequence, central Transantarctic Mountains, Antarctica: zircon geochronology, provenance, and basin evolution. Geosphere 13 (1), 155–178.
Elliot, D.H., Fanning, C.M., Mukasa, S.B., Millar, I.L., 2019. Hf-and O-isotope data from detrital and granitoid zircons reveal characteristics of the Permian–Triassic magmatic belt along the Antarctic sector of Gondwana. Geosphere 15 (2), 576–604. https://doi.org/10.1130/GES02011.1.
Elsner, M., Schöner, R., Gerdes, A., Gaupp, R., 2013. Reconstruction of the early Mesozoic plate margin of Gondwana by U-Pb ages of detrital zircons from northern. In: Harley, S.L., Fitzsimons, I.C.W., Zhao, Y. (Eds.), Antarctica and Supercontinent Evolution: Geological Society of London Special Publication, 383, pp. 211–232. https://doi.org/10.1144/SP383.5.
Estrada, S., Läufer, A., Eckelmann, K., Hofmann, M., Gärtner, A., Linnemann, U., 2016. Continuous Neoproterozoic to Ordovician sedimentation at the East Gondwana margin—Implications from detrital zircons of the Ross Orogen in northern Victoria Land, Antarctica. Gondwana Res. 37, 426–448.
Fitzgerald, P.G., 1992. The Transantarctic Mountains of southern Victoria Land: the application of apatite fission track analysis to a rift shoulder uplift. Tectonics 11 (3), 634–662.
Fitzgerald, P.G., 2002. Tectonics and landscape evolution of the Antarctic plate since the breakup of Gondwana, with an emphasis on the West Antarctic Rift System and the Transantarctic Mountains. Royal Soc. N. Z. Bull. 35, 453–469.
Fitzgerald, P.G., Baldwin, S., 1997. Detachment fault model for evolution of the Ross Embayment. In: Ricci, C.A. (Ed.), The Antarctic region: Processes and evolution: Siena, Terra Antartica Publications, pp. 555–564.
Ford, A.B., Barrett, P.J., 1975. Basement rocks of the south-Central Ross Sea, Site 270, DSDP Leg 28. In: Hayes, D.E., Frakes, I.A., et al. (Eds.), Initial Reports of the Deep Sea Drilling Project. U.S. Government Printing Office, Washington, D.C.. https://doi.org/10.2973/dsdp.proc.28.131.1975
Fretwell, P., et al., 2013. Bedmap2: improved ice bed, surface and thickness datasets for Antarctica. Cryosphere 7, 375–393.
Gleadow, A.J.W., Duddy, I.R., 1981. A natural long-term track annealing experiment for apatite. Nucl. Tracks 5 (1), 169–174.
Goodge, J.W., 2020. Geological and tectonic evolution of the Transantarctic Mountains, from ancient craton to recent enigma. Gondwana Res. 80, 50–122.
Goodge, J.W., Williams, I.S., Myrow, P., 2004. Provenance of Neoproterozoic and lower Paleozoic siliciclastic rocks of the Central Ross orogen, Antarctica: Detrital record of rift-, passive-, and active-margin sedimentation. Geol. Soc. Am. Bull. 116, 1253–1279. https://doi.org/10.1130/B25347.1.
Hagen-Peter, G., Cottle, C., 2016. Synchronous alkaline and subalkaline magmatism during the late Neoproterozoic–early Paleozoic Ross orogeny, Antarctica: Insights into magmatic sources and processes within a continental arc. Lithos 262, 677–698.
Jamieson, S.S., Sugden, D.E., Hulton, N.R., 2010. The evolution of the subglacial landscape of Antarctica. Earth Planet. Sci. Lett. 293 (1–2), 1–27.
Jordan, T.A., Riley, T.R., Siddoway, C.S., 2020. The geological history and evolution of West Antarctica. Nature Rev. Earth & Environ. 1 (2), 117–133.
Kraus, C., 2016. Oligocene to Early Miocene Glacimarine Sedimentation of the Central Ross Sea, and Implications for the Evolution of the West Antarctic Ice Sheet. Victoria University of Wellington, p. 164 (Unpublished MSc. Thesis).
Kulhanek, D.K., Levy, R.H., Clowes, C.D., Prebble, J.G., Rodelli, D., Jovane, L., Naish, T. R., 2019. Revised chronostratigraphy of DSDP Site 270 and late Oligocene to early Miocene paleoecology of the Ross Sea sector of Antarctica. Glob. Planet. Chang. 178, 46–64.
Leckie, R.M., Webb, P.-N., 1983. Late Oligocene–early Miocene glacial record of the Ross Sea, Antarctica : evidence from DSDP Site 270. Geology 11, 578–582.
LeMasurier, W., 2013. Shield volcanoes of Marie Byrd Land, West Antarctic rift: oceanic island similarities, continental signature, and tectonic controls. Bull. Volcanol. 75, 726.
Levy, R.H., et al., 2019. Antarctic ice-sheet sensitivity to obliquity forcing enhanced through ocean connections. Nat. Geosci. 12, 132–137.
Li, X., Zattin, M., Olivetti, V., 2020. Apatite fission track signatures of the Ross Sea ice flows during the Last Glacial Maximum. Geochem. Geophys. Geosyst. 21, e2019GC008749.
Licht, K.J., Hemming, S.R., 2017. Analysis of Antarctic glacigenic sediment provenance through geochemical and petrologic applications. Quat. Sci. Rev. 164, 1–24.
Licht, K.J., Palmer, E.F., 2013. Erosion and transport by Byrd Glacier, Antarctica during the last glacial maximum. Quat. Sci. Rev. 62, 32–48.
Licht, K.J., Hennessy, A.J., Welke, B.M., 2014. The U-Pb detrital zircon signature of West Antarctic ice stream tills in the Ross embayment, with implications for last Glacial Maximum ice flow reconstructions. Antarct. Sci. 26 (6), 687–697.
Mark, C., Cogné, N., Chew, D., 2016. Tracking exhumation and drainage divide migration of the Western Alps: a test of the apatite U-Pb thermochronometer as a detrital provenance tool. GSA Bull. 128 (9–10), 1439–1460.
Marschalek, J.W., Zurli, L., Talarico, F., van de Flierdt, T., Vermeesch, P., Carter, A., Beny, F., Bout-Roumazeilles, V., Sangiorgi, F., Hemming, S.R., Pérez, L.F., Colleoni, F., Prebble, J.G., van Peer, T.E., Perotti, M., Shevenell, A.E., Browne, I., Kulhanek, D.K., Levy, R., Harwood, D., Sullivan, N.B., Meyers, S.R., Griffith, E.M., Hillenbrand, C.-D., Gasson, E., Siegert, M.J., Keisling, B., Licht, K.J., Kuhn, G., Dodd, J.P., Boshuis, C., De Santis, L., McKay, R., M. & IODP Expedition 374, 2021. A large West Antarctic Ice Sheet explains early Neogene Sea-level amplitude. Nature 600 (7889), 450–455.
McFadden, R.R., Siddoway, C.S., Teyssier, C., Fanning, C.M., 2010. Cretaceous oblique extensional deformation and magma accumulation in the Fosdick Mountains migmatite-cored gneiss dome, West Antarctica. Tectonics 29 (4).
McKay, R.M., De Santis, L., Kulhanek, D.K., Browne, I.M., Shevenell, A.E., 2019. Site U1521.
Millar, I.L., Pankhurst, R.J., 1987. Gondwana Six: Structure, Tectonics, and Geophysics Vol. 40 (ed. McKenzie, G. D.) 151–160 (American Geophysical Union, 1987).
Mortimer, N., Palin, J.M., Dunlap, W.J., Hauff, F., 2011. Extent of the Ross Orogen in Antarctica: new data from DSDP 270 and Iselin Bank. Antarct. Sci. 23 (3), 297–306.
Naish, T.R., Duncan, B., Levy, R., McKay, R.M., Escutia, C., De Santis, L., Colleoni, F., Gasson, E.G.W., DeConto, R.M., Wilson, G., 2022. Antarctic Ice Sheet dynamics during the late Oligocene and early Miocene: Climatic conundrums revisited. In: Antarctic Climate Evolution. Elsevier, pp. 363–387.
Olivetti, V., Balestrieri, M.L., Chew, D., Zurli, L., Zattin, M., Pace, D., Drakou, F., Cornamusini, G., Perotti, M., 2023. Detrital age spectra and petrological analysis of gravel-size clasts of the Oligocene-early Miocene glaciomarine sediments of the DSDP drilling Site 270, Central Ross Sea, Antarctica. GFZ Data Services. 10.5880/fidgeo.2022.040.
Olivetti, V., Balestrieri, M.L., Rossetti, F., Talarico, F.M., 2013. Tectonic and climatic signals from apatite detrital fission track analysis of the Cape Robert Project core records, South Victoria Land, Antarctica. Tectonophysics 594, 80–90. https://doi.org/10.1016/j. tecto.2013.03.017.
O'Sullivan, G., Chew, D., Kenny, G., Henrichs, I., Mulligan, D., 2020. The trace element composition of apatite and its application to detrital provenance studies. Earth-Sci. Rev. 201, 103044.
O'Sullivan, G.J., Chew, D.M., Samson, S.D., 2016. Detecting magma poor orogens in the detrital record. Geology 44 (10), 871–874. https://doi.org/10.1130/G38245.1.
O'Sullivan, G.J., Chew, D.M., Morton, A.C., Mark, C., Henrichs, I.A., 2018. An integrated apatite geochronology and geochemistry tool for sedimentary provenance analysis. Geochem. Geophys. Geosyst. 1309–1326 https://doi.org/10.1002/2017GC007343.
Pälike, H., Norris, R.D., Herrle, J.O., Wilson, P.A., Coxall, H.K., Lear, C.H., Shackleton, N. J., Tripati, A.K., Wade, B.S., 2006. The heartbeat of the Oligocene climate system. Science 314 (5807), 1894–1898.
Pankhurst, R.J., Weaver, S.D., Bradshaw, J.D., Storey, B.C., Ireland, T.R., 1998. Geochronology and geochemistry of pre-Jurassic superterranes in Marie Byrd Land, Antarctica. J. Geophys. Res. 103, 2529–2547.
Paton, C., Hellstrom, J., Paul, B., Woodhead, J., Hergt, J., 2011. Iolite: Freeware for the visualisation and processing of mass spectrometric data. J. Analytical Atomic Spectr. 26, 2508. https://doi.org/10.1039/c1ja10172b.
Paulsen, T., Deering, C., Sliwinski, J., Valencia, V., Bachmann, O., Guillong, M., 2017. Detrital zircon ages and trace element compositions of Permian–Triassic foreland basin strata of the Gondwanide orogen, Antarctica. Geosphere 13 (6), 2085–2093.
Paulsen, T.S., Encarnación, J., Grunow, A.M., Valencia, V.A., Layer, P.W., Pecha, M., Stump, E., Roeske, S., Thao, S., Rasoazanamparany, C., 2015. Detrital mineral ages from the Ross Supergroup, Antarctica: Implications for the Queen Maud terrane and outboard sediment provenance on the Gondwana margin. Gondwana Res. 27, 377–391. https://doi.org/10.1016/j.gr.2013.10.006.
Paxman, G.J.G., Jamieson, S.S.R., Hochmuth, K., Gohl, K., Bentley, M.J., Leitchenkov, G., Ferraccioli, F., 2019. Reconstructions of Antarctic topography since the Eocene-Oligocene boundary. Palaeogeogr. Palaeoclimatol. Palaeoecol. 535, 109346 https://doi.org/10.1016/j.palaeo.2019.109346.
Perotti, M., Andreucci, B., Talarico, F., Zattin, M., Langone, A., 2017. Multianalytical provenance analysis of E astern Ross Sea LGM till sediments (Antarctica): Petrography, geochronology, and thermochronology detrital data. Geochem. Geophys. Geosyst. 18 (6), 2275–2304.
Perotti, M., Zurli, L., Sandroni, S., Cornamusini, G., Talarico, F., 2018. Provenance of Ross Sea Drift in McMurdo Sound (Antarctica) and implications for middle-Quaternary to LGM glacial transport: New evidence from petrographic data. Sediment. Geol. 371, 41–54.
Petrus, J.A., Kamber, B.S., 2012. VizualAge: a novel approach to laser ablation ICP-MS U-Pb geochronology data reduction. Geostand. Geoanal. Res. 36, 247–270. https://doi.org/10.1111/j.1751-908X.2012.00158.x.
Pollard, D., DeConto, R.M., 2020. Continuous simulations over the last 40 million years with a coupled Antarctic ice sheet-sediment model. Palaeogeogr. Palaeoclimatol. Palaeoecol. 537, 109374.
Rocchi, S., Armienti, P., D'Orazio, M., Tonarini, S., Wijbrans, J.R., Di Vincenzo, G., 2002. Cenozoic magmatism in the western Ross Embayment: Role of mantle plume versus plate dynamics in the development of the West Antarctic Rift System. J. Geophys. Res. 107 https://doi.org/10.1029/2001JB000515.
Shipboard Scientific Party, 1975. Sites 270, 271, 272. In: Hayes, D.E., Frakes, L.A. (Eds.), Initial Reports of the Deep Sea Drilling Project, vol. 28. U.S. Government Printing Office, Washington, pp. 211–334.
Siddoway, C., 2008. Tectonics of the West Antarctic Rift System: New light on the history and dynamics of distributed intracontinental extension. In: Cook, A.K., Barrett, P., Stagg, H., Storey, B., Stump, E., Wise, W. (Eds.), Antarctica: A Keystone in a Changing World: Washington. The National Academic Press, DC, pp. 91–114.
Siddoway, C.S., 2021. Geology of West Antarctica. Beiträge zur regionalen Geologie der Erde, p. 33.
Siddoway, C.S., Baldwin, S., Fitzgerald, G., Fanning, C.M., Luyendyk, B.P., 2004. Ross Sea mylonites and the timing of intracontinental extension within the West Antarctic rift system. Geology 32, 57–60.
Stacey, J.S., Kramers, J.D., 1975. Approximation of terrestrial lead isotope evolution by a two-stage model: Earth and Plan. Sci. Lett. 26, 207–221. https://doi.org/10.1016/0012-821X(75)90088-6.
Stump, E., 1995. The Ross Orogen of the Transantarctic Mountains. Cambridge University Press.
Talarico, F.M., Sandroni, S., 2011. Early Miocene basement clasts in ANDRILL AND-2A core and their implications for paleoenvironmental changes in the McMurdo Sound region (western Ross Sea, Antarctica). Glob. Planet. Chang. 78 (1–2), 23–35.

Talarico, F.M., McKay, R.M., Powell, R.D., Sandroni, S., Naish, T., 2012. Late Cenozoic oscillations of Antarctic ice sheets revealed by provenance of basement clasts and grain detrital modes in ANDRILL core AND-1B. Glob. Planet. Chang. 96, 23–40.

Tinto, K.J., Padman, L., Siddoway, C.S., Springer, S.R., Fricker, H.A., Das, I., et al., 2019. Ross Ice Shelf response to climate driven by the tectonic imprint on seafloor bathymetry. Nat. Geosci. 12 (6), 441–449. https://doi.org/10.1038/s41561-019-0370-2.

Veevers, J.J., 2004. Gondwanaland from 650–500Ma assembly through 320 Ma merger in Pangea to 185–100 Ma breakup: supercontinental tectonics via stratigraphy and radiometric dating. Earth-Sci. Rev. 68, 1–132.

Vermeesch, P., 2012. On the visualisation of detrital age distributions. Chem. Geol. 312, 190–194.

Vermeesch, P., 2013. Multi-sample comparison of detrital age distributions. Chem. Geol. 341, 140. https://doi.org/10.1016/j.chemgeo.2013.01.010.

Wilson, D.S., Jamieson, S.S.R., Barrett, P.J., Leitchenkov, G., Gohl, K., Larter, R.D., 2012. Antarctic topography at the Eocene-Oligocene boundary. Palaeogeogr. Palaeoclimatol. Palaeoecol. 335–336, 24–34.

Yakymchuk, C., Brown, C.R., Brown, M., Siddoway, C.S., Fanning, C.M., Korhonen, F.J., 2015. Paleozoic evolution of western Marie Byrd Land, Antarctica. Geol. Soc. Am. Bull. 127, 1464–1484. https://doi.org/10.1130/B31136.1.

Zundel, M., Spiegel, C., Mehling, A., Lisker, F., Hillenbrand, C.D., Monien, P., Klügel, A., 2019. Thurston Island (West Antarctica) between Gondwana subduction and continental separation: a multistage evolution revealed by apatite thermochronology. Tectonics 38 (3), 878–897.

Zurli, L., Cornamusini, G., Woo, J., Liberato, G.P., Han, S., Kim, Y., Talarico, F.M., 2022a. Detrital zircons from late Paleozoic Ice Age sequences in Victoria Land (Antarctica): New constraints on the glaciation of southern Gondwana. GSA Bull. 134, 160–178. https://doi.org/10.1130/B35905.1.

Zurli, L., Perotti, M., Talarico, F.M., 2022b. Data report: petrology of gravel-sized clasts from Site U1521 core, IODP Expedition 374, Ross Sea West Antarctic Sheet history. In McKay, R.M., De Santis, L., Kulhanek, D.K., the Expedition 374 scientists, Ross Sea West Antarctic Ice Sheet history. Proceedings of the International Ocean Discovery Program, 374: College Station, TX (International Ocean Discovery Program). doi: 10.14379/iodp.proc.374.201.2022.

Further reading

Weaver, S.D., Bradshaw, J.D., Adams, C.J., 1991. Granitoids of the Ford Ranges, Marie Byrd Land, Antarctica. In: Thomson, M.R.A., Crame, J.A., Thomson, J.W. (Eds.), Geological Evolution of Antarctica. Cambridge University Press, Cambridge, pp. 345–351.